JOURNAL OF Applied Polymer SCIENCE

Structural and Morphological Development in Polypropylene/Poly(propylene-1-octene) In-Reactor Alloy Due to the Competition Between Liquid–Liquid Phase Separation and Crystallization

Jihui Wang,[1,2] Charles C. Han[1]

[1]State Key Laboratory of Polymer Physics and Chemistry, Chinese Academy of Sciences, Beijing 100190, China

[2]Graduate School of the Chinese Academy of Sciences, Beijing 100190, China

Correspondence to: C. C. Han (E-mail: c.c.han@iccas.ac.cn)

ABSTRACT: Relationship between phase separation and crystallization of polypropylene/poly(propylene-1-octene) in-reactor alloy (iPP/PPOc) were studied using optical microscopy, scanning electron microscopy, and differential scanning calorimetry. Optical microscopy was used to monitor nuclei density and spherulite growth rates, providing complementary information about the effect of liquid–liquid phase separation (LLPS) on crystallization behavior. We found that LLPS process had a retardation effect on crystallization rate and had a dominant effect on the final crystalline morphology of the iPP/PPOc alloy. By simply changing the LLPS time or temperature, we could control the size and the distribution of the elastomer phase that dispersed in the iPP spherulites. The growth rate of the spherulites significantly depended on the degree of LLPS. Higher degree of phase separation reduced nuclei density and the growth rate of spherulites. However, it was helpful to the formation of more perfect spherulites. But surprisingly, there seemed to be little variation of crystallinity between the two quenching procedures (i.e., single quench vs. double quench). Overall, the competition between LLPS and crystallization significantly influenced the structural and morphological development of the iPP/PPOc alloy. By controlling the interplay between LLPS and crystallization of iPP/PPOc alloy, it was possible to control the structure and morphology as needed in applications. © 2013 Wiley Periodicals, Inc. J. Appl. Polym. Sci. 129: 2977–2985, 2013

KEYWORDS: crystallization; Kinetics; Morphology; phase behavior; polyolefins

Received 10 September 2012; accepted 10 January 2013; published online 15 February 2013

DOI: 10.1002/app.39030

INTRODUCTION

Polypropylene (PP) in-reactor alloys have been widely used to modify iPP to improve the low temperature impact strength.[1,2] A clear understanding of the fundamental physics of these polymers is essential to control the specific compounding and manufacturing processes. The majority of published literatures are related to the homopolymerization of ethylene or propylene, and the copolymerization of ethylene with higher α-olefins. However, it has been reported that even small amounts of 1-hexene or 1-octene can provide the synthesis of PP with low density and improved processability.[3] Therefore, more and more recent studies are devoted to the copolymerization of propylene with higher α-olefins.[4–6]

The melt miscibility of polyolefin blends has long been a challenging subject because the constituting components have similar chemical structures and very close refractive indices, which made it difficult to determine whether an observed transparent sample is truly in a "homogeneous state" or not.[7–9] The properties of PP alloys are determined not only by miscibility (or compatibility) between the components, but also depend to a large extent on their crystalline structure, therefore many research papers have been published on the morphology and kinetics of crystallization in blends.[10–17] Some studies have been reported on the compositional heterogeneity, chain structure, and properties of the in-reactor-prepared PP alloys.[18–21] However, very few articles were actually focused on the relationship of liquid–liquid phase separation (LLPS) and crystallization of this kind of polymer alloy.[22,23]

Our research interest is in monitoring the LLPS process in a crystalline-amorphous blend via crystallization kinetics and phase morphology. As is well known, the morphology of the blends has a great effect on their properties.[24–26] The excellent properties of PP-based in-reactor alloy depend very much on the special nascent micro- and nanoscale phase structure. It is necessary to study the phase separation, the crystalline morphology, crystallization kinetics, and mechanism thoroughly to be able to control the final properties through the control of the structure and morphology. Therefore, a two-step process was specifically designed such that liquid–liquid phase

separation occurred before crystallization. The first step is to isothermally anneal the alloy to reach a certain phase-separated state at temperatures above the melting temperature of the crystalline phase to avoid crystallization. This leaves the phase morphology in a particular phase state.[27] In the second step, the sample is isothermally or nonisothermally crystallized by quenching to a lower temperature where crystallization occurs. Further concentration changes in the phase domains are minimal because of the rate of crystallization is normally much faster.

In this article, we presented a systematic study on the characteristic phase separation, crystalline morphology, and the LLPS effect on the crystallization behavior of a special two catalysts and one reactor formed iPP/PPOc in-reactor alloy[28] by polarized optical microscope, phase contrast optical microscope, differential scanning calorimetry (DSC), and scanning electron microscope (SEM) methods. The LLPS process provided systematic control over the final crystalline morphology. Based on experimental results, several new insights into the interplay between the LLPS and crystallization for the iPP/PPOc alloy were obtained.

EXPERIMENTAL

Samples and Preparation

A one-step polymerization process was conducted using high-activity $MgCl_2$-$TiCl_4$/rac-Me_2-Si(Ind)$_2ZrCl_2$ hybrid catalyst.[29] The nascent polypropylene/poly(propylene-1-octene) (iPP/PPOc) particles were directly obtained in reactor after this preparation of one polymerization process in one reactor.[28] The weight-average molecular mass was 4.9×10^5, and the polydispersity index (weight-average molecular mass/number-average molecular mass) of the blend was 4.2, measured by gel permeation chromatograph (GPC). The atactic fraction of polymers was measured by extracting the polymers for 12 h with boiling *n*-heptane in a Soxhlet-type apparatus. The average elastomer content of the iPP/PPOc particles was 40 wt % (PPOc40).

Morphology Investigation

Nucleation and growth processes of spherulites in iPP/PPOc alloy during isothermal crystallization were recorded in real-time using a Nikon polarized optical microscope equipped with a Kodak Megaplus charge coupled device (CCD) camera. During crystallization, growth of the spherulites was monitored as a function of time and the linear growth rate of spherulites was determined from the slope in the plots of spherulite radius versus time. The blend particles were hot-pressed at 210°C to form films of 20 μm in thickness (for optical microscopy) and then quenched to room temperature for further use.

The samples after optical microscopy test were etched in *n*-heptane at ambient temperature for 1 week to wash out the more soluble component (propylene-1-octene random copolymer), and then the film was coated with platinum before examination by SEM. A JEOL (JSM 6700F) SEM was used with an operating voltage of 5 kV for this study.

DSC Analysis

A TA Q2000 DSC apparatus was used for the determination of the thermal properties of iPP/PPOc in-reactor alloys. About 4–6 mg of the sample was used and sealed in an aluminum pan. The calibration of the temperature scale and the heat flow was achieved from the melting scans of high-purity indium and zinc samples at the same heating rate. The thermal history of the samples was eliminated by holding at 210°C for 5 min. Subsequently, the samples were quenched to LLPS temperature for certain time, and then cooled to 40°C at a rate of 10°C/min. The melting temperature and fusion enthalpy of the samples were determined during the second heating scan at a rate of 10°C/min.

RESULTS AND DISCUSSION

Successive self-nucleation and annealing (SSA) is an effective thermal fractionation method, which is based on the sequential application of self-nucleation and annealing steps on polymer samples. It can give information on the distribution of short chain branching and lamellae thickness.

The SSA method is used as presented in the original article by Muller et al.[30] The self-seeding temperature (T_s), which is thought to be one of the most important parameters in SSA research, was suggested by Mueller to be the minimum temperature of melting domains, in which the temperature is high enough to melt almost all of the polymer crystals but low enough to leave "small" crystal fragments that can act as self-nuclei. The first T_s was chosen based on the final melting temperature of the melting curve, as shown in Figure 1(a). The annealing time (t_s) was kept at 15 min at each step. Figure 1 shows the melting trace of the sample after having been subjected to an eight-step SSA treatment with a decrease of 5°C per step from 145 to 110°C (145, 140, 135, 130, 125, 120, 115, 110°C). The appearance of seven major melting peaks in the curve indicates that thermal fractionation has occurred during the SSA treatment and each peak should correspond to the melting of a particular lamellar population. The fractions that exhibit the highest melting points at 147.2°C are those with the longest linear or isotactic segments incorporated within the specific lamellar population, and therefore, they should be the ones with the lowest defects concentration.[31] The lamellae thickness of the crystals has a wide distribution because the polymer chains are heterogeneous. The crystalline PP segments in the blocky copolymer fractions are chemically linked with other segments (such as propylene–octene random copolymer segments); leading to the lower melting temperature of PP segments.[32,33] Peaks also could due to different diffusion coefficient or kinetics. It should also be noted that the SSA technique only detects the defects distribution of propylene sequences long enough to crystallize, and the sequences too short to crystallize cannot be detected.[34]

Figure 1(a) presents the cooling and heating curves of the sample without SSA process. The melting point and crystallization temperature were shown in Figure 1(a). After SSA process, the next cooling and subsequently heating curves were also shown in Figure 1(b). If we compare the crystallization curve and melting temperature of the samples before and after SSA process, we could find that the crystallization and melting peaks (including temperature and enthalpy) almost have no change, which

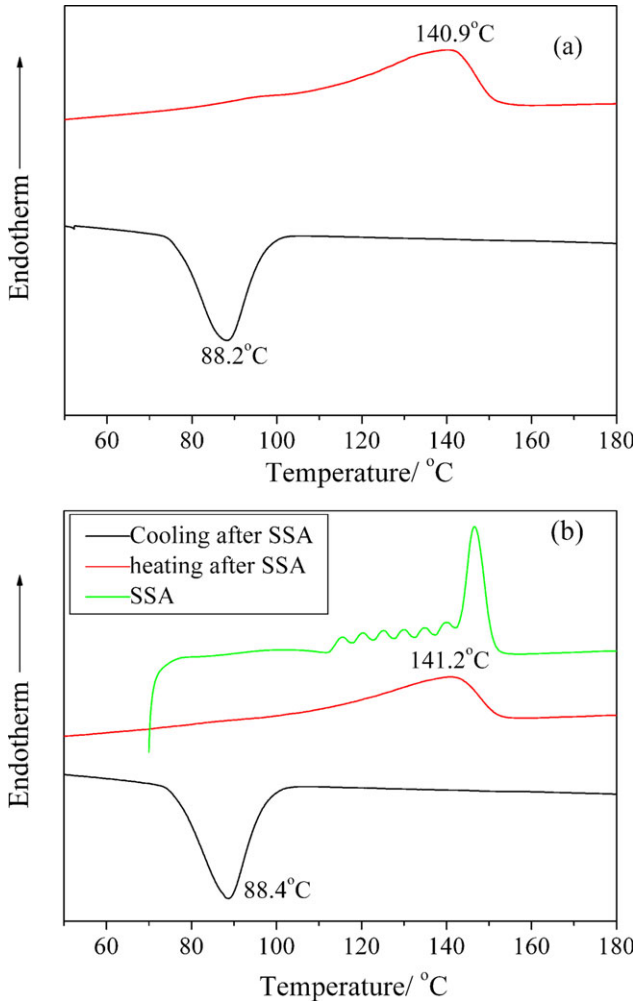

Figure 1. DSC cooling and heating curves for PPOc40 sample before (a) and after SSA, with a fractionation window of 5°C and the subsequent cooling and heating curves (b). [Color figure can be viewed in the online issue, which is available at wileyonlinelibrary.com.]

indicated that the multiple peaks could due to different diffusion coefficient or kinetics also.

In the present system, phase contrast optical microscope could not provide the real space morphology evolution and the coarsening of the phase domains of iPP/PPOc alloy in the molten state due to the similar chemical structures and very close refractive indices of the components; therefore, the SEM images were used to offer an indirect proof of the morphology development by etching off the elastomer phase. Figure 2 represents the time dependence of morphology development during phase separation process. Phase separation was caused by segregation mainly between the crystallizable iPP and elastomer phase PPOc. According to the component proportion, the dispersed phase, namely, the droplets, should be the PPOc-rich phase, and the continuous phase should be the iPP-rich phase. To clarify this, a solvent etching technique was used. Samples were heated to 210°C to erase thermal history first. Then they were annealed at 160°C for LLPS for different times (t = 0, 4, 8, and 16 h). As iPP crystal cannot be dissolved in n-heptane at room temperature, whereas elastomer phase PPOc can be dissolved, the quenched samples were dipped into excessive n-heptane at room temperature for about 72 h for selective etching. After the elastomer component was removed from the sample by washing, spherical shaped cavities appeared on the surface of the sample. These globular cavities should be left by the droplets which had been etched out by solvent. It was clear now that the PPOc-rich phase formed the droplets.

It was obvious that the size of dispersed phase increased gradually with LLPS time, indicating the thermodynamic tendency of moving toward an equilibrium state; meanwhile, their size distribution was broadened.

To detect the effect LLPS temperature on the "droplet" size, the phase separation temperature was kept at T = 150, 160, 170, and 180°C for 16 h before quenched to room temperature. The quenched samples were dipped into excessive n-heptane at room temperature for about 72 h for selective etching. After the elastomer PPOc component was removed from the sample by washing, spherical shaped cavities appeared on the surface of the sample as shown in Figure 3. It showed that the globular cavities became smaller in size and the distribution became more uniform with the increase of LLPS temperature. At the LLPS temperature of 150°C (T_m = 140°C), big droplets size was about 1–2 μm and the small droplets size was about 0.5 μm. That might be due to the late stage coarsening effect. At the LLPS temperature 160°C, droplets size was about 0.5–1 μm. If we continuously increased the LLPS temperature, the droplets size became smaller. A characteristic phase domain size decreased with the increase of LLPS temperature. This indicates that the iPP/PPOc alloy has an upper critical solution temperature (UCST) type of phase behavior in the melt.

Figure 4(a) shows the nonisothermal crystallization behavior of the specimens, which were cooled down to 40°C at 10°C/min after LLPS at 160, 170, and 180°C for 8 h. A measurement for the sample cooled from 210 to 40°C without annealing was also provided for comparison. As shown in Figure 4(a), all the samples showed a reduced nucleation process compared to the sample without annealing. Figure 4(b) presents the relative crystallinity increase of different samples with time which were obtained by computing the area beneath the nonisothermal crystallization runs from a baseline over an interval of crystallization time. The baseline at the start of the crystallization run was extrapolated by a straight line and met at the end line. The total crystallization rate after the induction time of nucleation changed visibly with different LLPS temperature. It was obvious that the crystallization rate became more quickly with the increase of LLPS temperature. In contrast, the sample without LLPS process showed the fastest crystallization rate. This also indicated that the iPP/PPOc alloy exhibited a UCST phase behavior. It could be concluded that the crystallization kinetics had a strong dependence on phase separation temperature and annealing time.

Conventional DSC measurement was performed to further illustrate the effect of LLPS time on crystallization as shown in Figure 5. A clear reduction of the crystallization temperature was found with the increase of LLPS time as shown in Figure

Applied Polymer SCIENCE

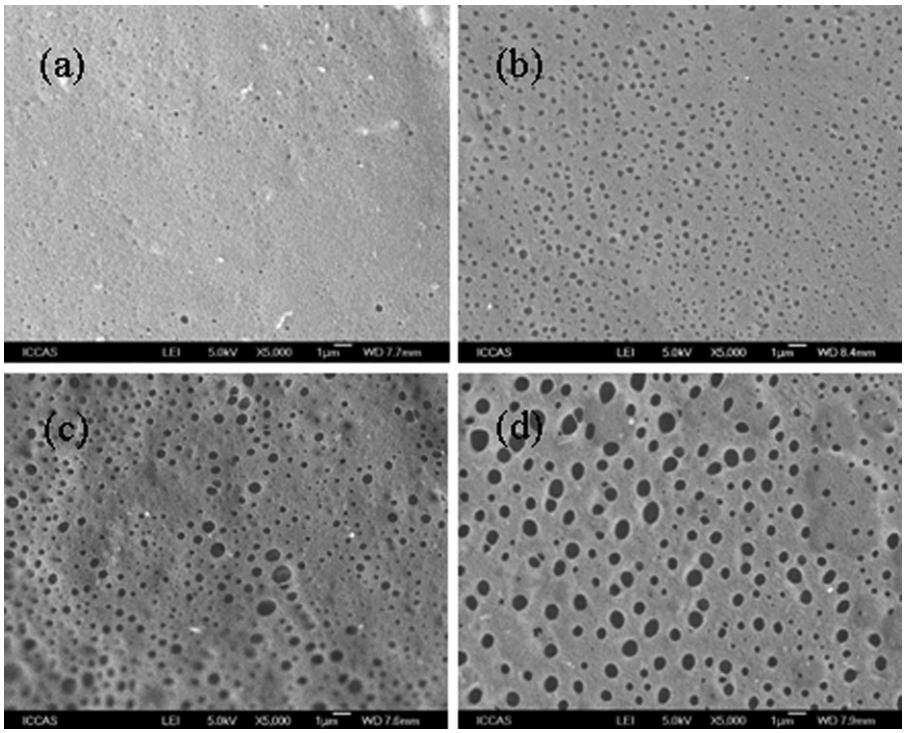

Figure 2. SEM images of the samples undergoing LLPS at 160°C for (a) 0, (b) 4, (c) 8, and (d) 16 h, followed by rapidly quenching to room temperature and solvent etching.

5(a). The entire specimen almost had similar onset crystallization temperature; however, it was obvious that the offset crystallization temperature became lower with in increase of LLPS time, which indicated that the crystallization time became longer with the increase of LLPS time. Faster nucleation effect from the interface region of these phase-separated domains occurred and higher apparent crystallization temperature (T_c) was observed for the sample without or with a short LLPS time.

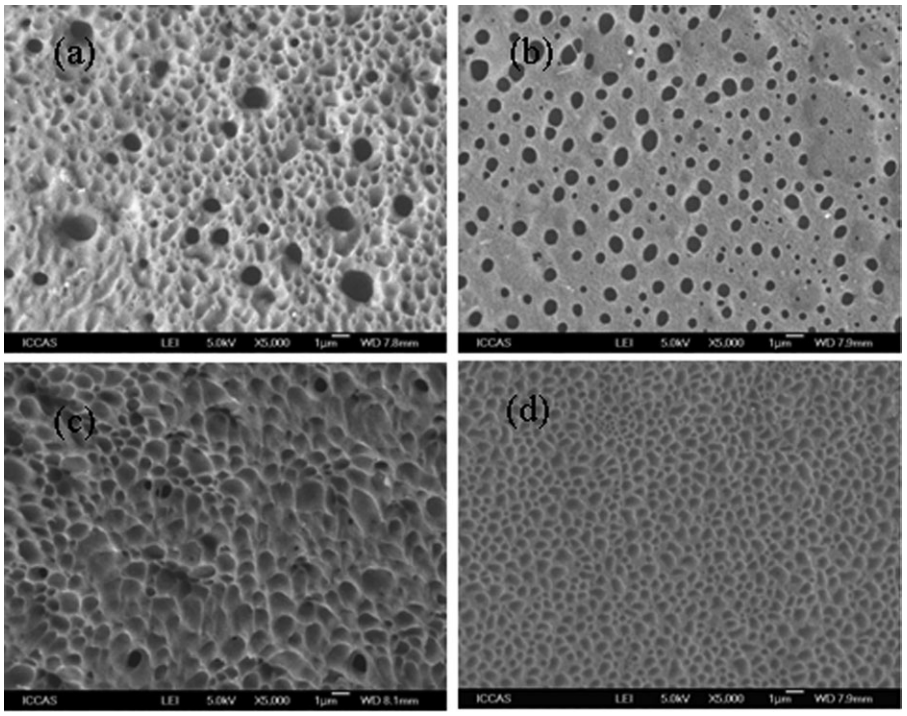

Figure 3. SEM images of the samples undergoing LLPS 16 h at different temperature for (a) 150, (b) 160, (c) 170, and (d) 180°C, followed by rapidly quenching to room temperature and solvent etching.

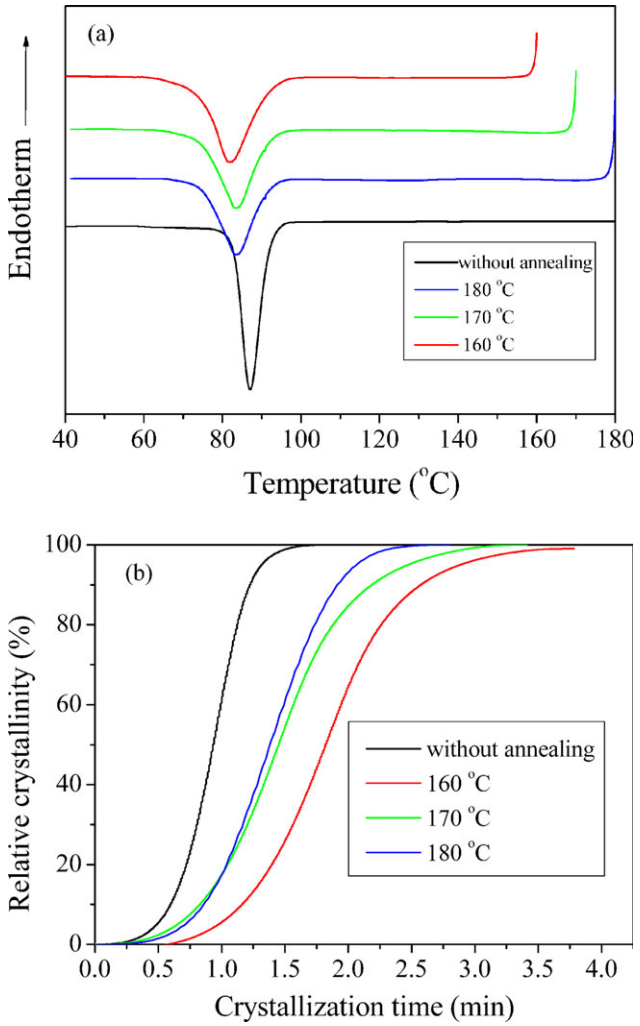

Figure 4. DSC cooling thermograms of the sample at a cooling rate 10°C/min, followed by different LLPS temperature for 160, 170, and 180°C. [Color figure can be viewed in the online issue, which is available at wileyonlinelibrary.com.]

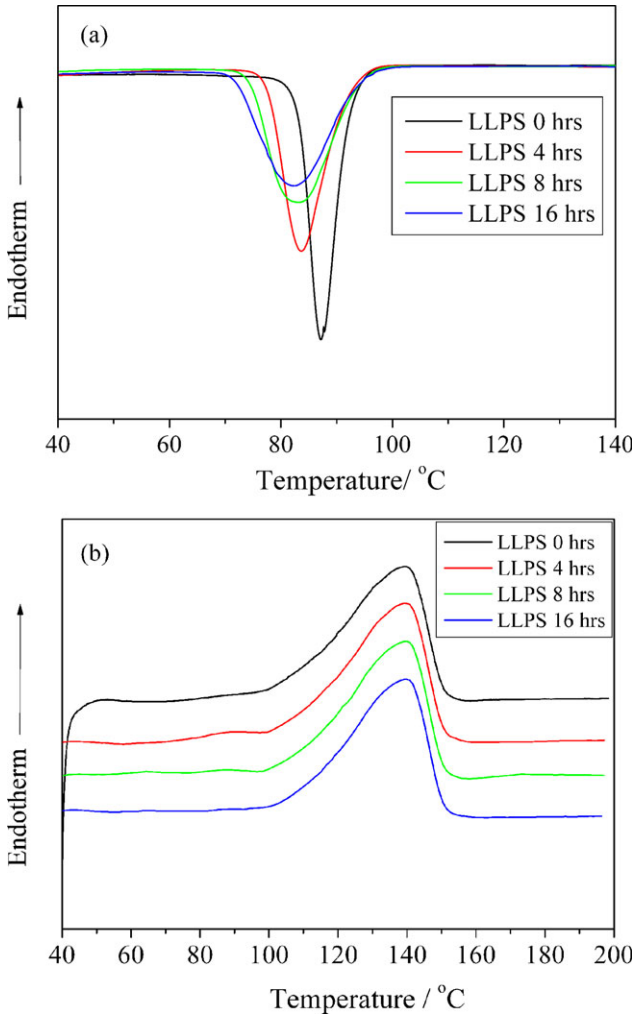

Figure 5. DSC cooling and heating thermograms after different LLPS time at 160°C. [Color figure can be viewed in the online issue, which is available at wileyonlinelibrary.com.]

The detailed results estimated by the DSC curves in Figure 5 were summarized in Table I. The crystallinity (X_c) was calculated from eq. (1) by assuming the heat of fusion of 100% crystalline PP ($\Delta H_{f\ -\ \mathrm{PP}}$) as 165 J/g.

$$X_c = \frac{\Delta H_f}{\Delta H_{f-\mathrm{PP}}} \times 100\% \quad (1)$$

Table I lists crystallization and melting temperature, crystallinity obtained during cooling, and subsequent heating scans at 10°C/min after LLPS at 160°C for different periods of time. As shown in Table I, the crystallinity and melting points of the samples almost unchanged with the increase of LLPS time at 160°C.

We have already known that the LLPS process had a retardation effect on crystallization behavior. Nuclei density and/or nucleation rate of the sample decreased obviously with the increase of LLPS time from Figures 6 and 7. It was postulated that the decreased nuclei density and/or nucleation rate followed the fluctuation-assisted nucleation mechanism: the enhanced concentration fluctuation at the interfacial area played an important role in the nucleation behavior of iPP/PPOc alloys. The decreased interface areas with the increased LLPS time were responsible for lower nuclei density.[34,35]

The number of spherulites per unit area, determined by light microscopy from Figure 6, significantly decreased with the increase of LLPS time as shown in Figure 7. This implied that the concentration fluctuation due to early stage of phase separation (at the domain interface) could give rise to higher nuclei

Table 1. Effect of LLPS Time on Crystallization Temperature, Melting Temperature and Degree of Crystallinity

	LLPS time (h)			
	0	4	8	16
T_m (°C)	139.5	139.2	139.9	139.9
T_c (°C)	87.0	83.7	83.2	82.1
X_c (°C)	23.4	23.2	23.3	23.3

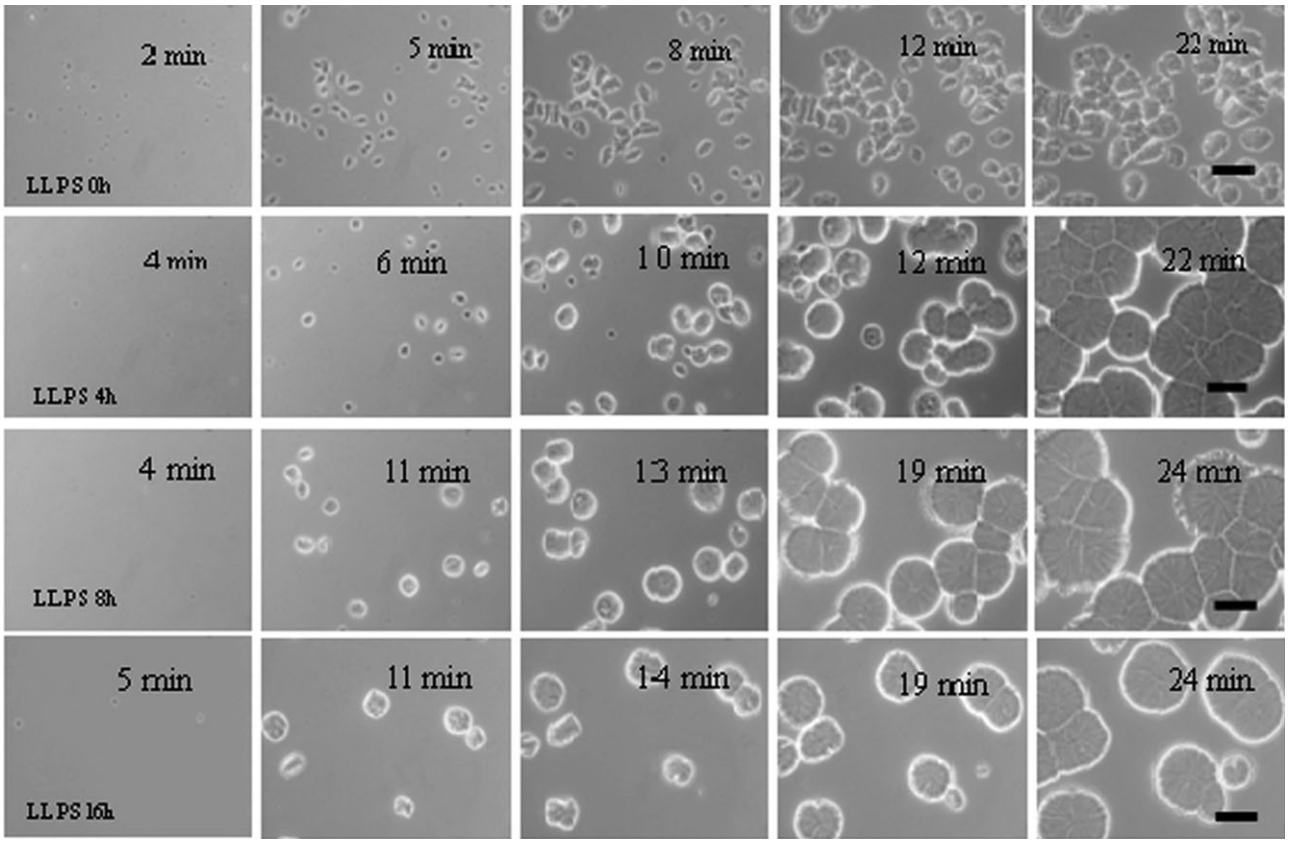

Figure 6. Phase contrast optical micrograph for samples after different phase separation at 160°C and then isothermally crystallized at 120°C. Bars correspond to 50 μm.

density or nucleation rate. The decrease in number of crystallized spherulite associated with the increase of LLPS and the predominance of nuclei near the domain interface could be explained by the fact that the interfacial region of a phase separating system was favorable for the nucleation process, which could be observed from the appearance of nuclei and the number of nuclei. This was because the longer the time spent in LLPS after the first quench, the sharper the total interface and the smaller the interfacial areas became, rendering it less probable that LLPS assisted nucleation would occur.

To rationalize the effect of the LLPS process on spherulite growth rates in miscible system, Figure 8 shows growth rate data of the samples as a function of LLPS time. They showed a time dependence of spherulite growth rate in the alloys. Where the amorphous component must diffuse out of spherulite in a direction normal to the growth direction or could be left behind into the interlamellar regions. The enrichment of the amorphous component in the interlamellar regions is confirmed by SEM. With the increase of LLPS time, the spherulite growth rate was decreased slightly. This phenomenon may be related to the relative ratio of diffusion rate of the amorphous component to the crystal growth rate.

Figure 9 shows the polarized optical microscopy (POM) micrographs of PP spherulites isothermally crystallized at 120°C after undergoing different LLPS time at 160°C. It could be seen that the morphologies of the specimens crystallized from the melts were always spherulitic. For the sample without LLPS process, spherulitic structure was very irregular as shown in Figure 9(a). Some dark regions were observed inside the spherulites, meaning that there existed the influence of propylene–octene copolymer on the crystalline structure of the alloy. As the amorphous domain between cross-polarized light is dark, the dark regions inside the spherulites may be the domains of the blocky

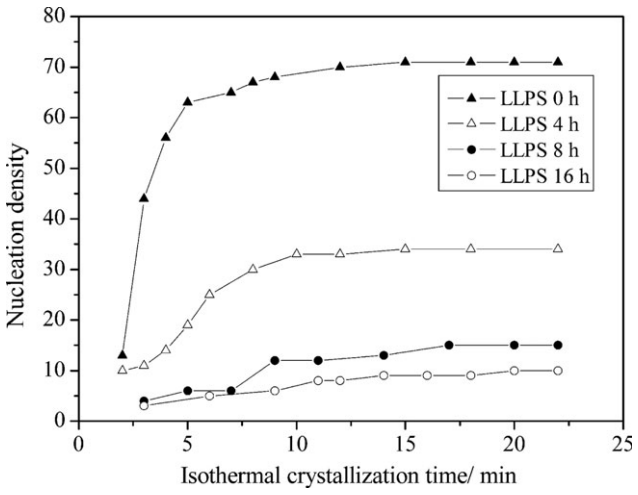

Figure 7. Number of spherulites per unit area as function of isothermal crystallization time at 120°C after LLPS at 160°C for different time.

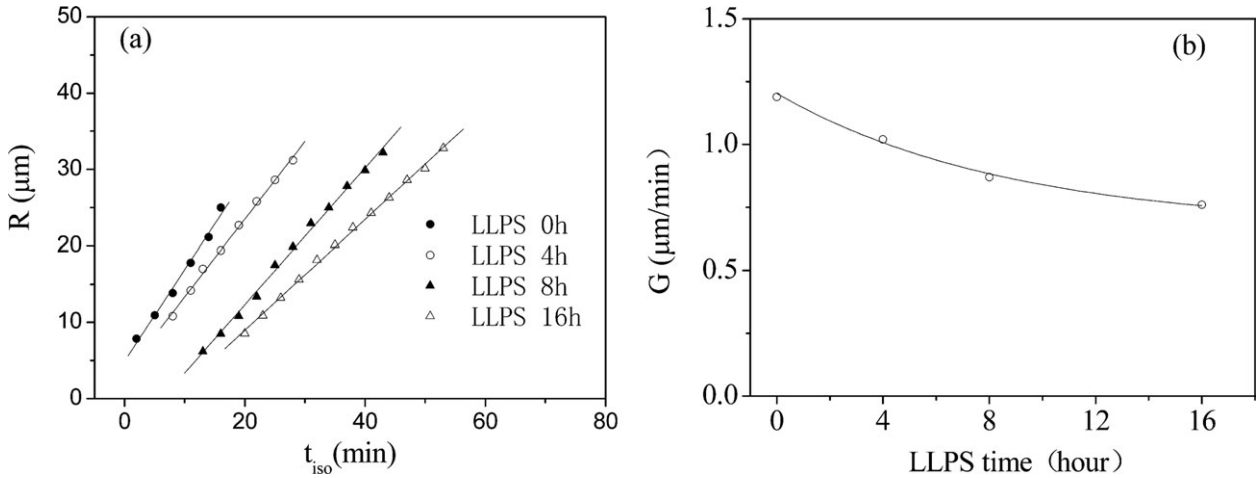

Figure 8. Growth rate of spherulites during isothermal crystallization at $T_c = 120°C$ with different LLPS time (a) and effect of LLPS time on spherulites growth rate (b).

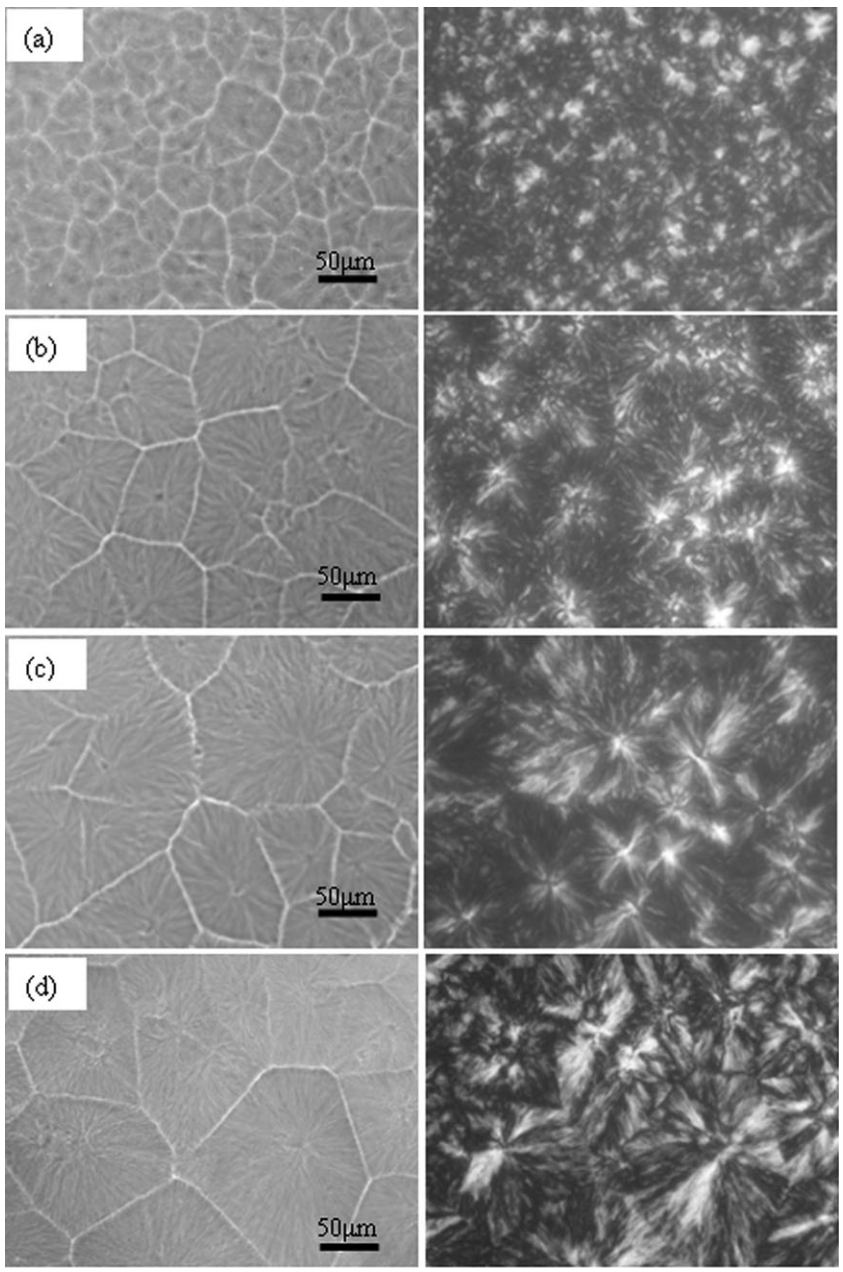

Figure 9. Polarized optical micrographs of the iPP spherulites isothermally crystallized at 120°C after undergoing different LLPS time at 160°C for (a) 0, (b) 4, (c) 8, and (d) 16 h, respectively.

Applied Polymer SCIENCE

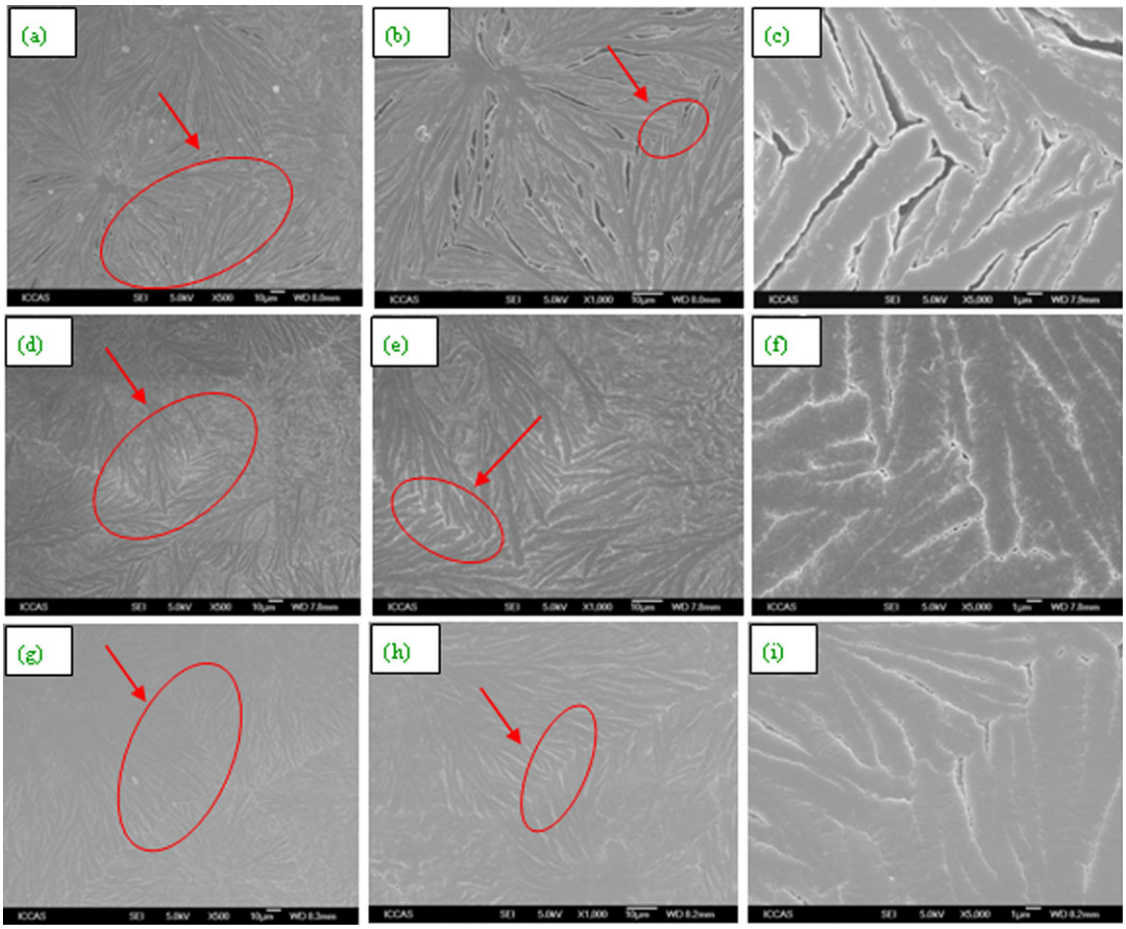

Figure 10. SEM images showing the morphological differences of the samples isothermally crystallized at 120°C after undergoing LLPS at 160°C for 0 h (a, b, c), 4 h (d, e, f), and 16 h (g, h, i). (c) are enlarged images from the circled areas in (a) and (b). And (f) are enlarged images from circled areas in (d) and (e). And (i) are enlarged images from circled areas in (g) and (h).The samples were etched by solvent. [Color figure can be viewed in the online issue, which is available at wileyonlinelibrary.com.]

fractions excluded from the PP matrix, which have much lower crystallinity when compared with the domains of neat PP. This phenomenon partly due to the small size of phase-separated domains and higher nuclei density. With the LLPS process for 4 h, spherulitic structure became perfect; however, negative birefringence was not observed obviously. The spherulites of samples after undergoing LLPS for 8 or 16 h at 160°C showed obviously negative birefringence, as shown in Figure 9(c,d). The spherulites compose of mainly radial lamellae because the cross-hatched structure is suppressed by LLPS process.[36–39] The transition from cross-hatched structure to radial lamellae of spherulitic structure could be achieved by the increase of LLPS time.

To see the final distribution of the crystal phase and the elastomer phase more clearly, three samples, crystallized at 120°C to the completion of spherulite growth after LLPS at 160°C for 0, 4, and 16 h, were dipped into *n*-heptane for 72 h to etch away the elastomer component and then observed by SEM. It could be seen that after solvent etching deep grooves appeared at the interfibrillar, as shown in Figure 10. These grooves were left by the PPOc-rich phase which had been etched out. The grooves between interfibrillar were much wider for the sample directly crystallized at 120°C without LLPS at 160°C, which implied that more elastomer components were accumulated at the interfibrillar regions. It was also observed that more elastomer PPOc component was trapped in the iPP spherulites and less was rejected outside the spherulites in the sample which had undergone LLPS at 160°C for 4 h before crystallization at 120°C, as shown in Figure 10(c,d). What unexpected is that there was no obvious spherulite boundaries as shown in Figure 10(e,f), which implied that the crystal component could link with each other for different spherulites and the elastomer phase were almost all left behind in the spherulite as droplets. It was very clearly that as the annealing time was increase from 0 to 16 h for LLPS, the grooves at the interfibrillar spaces became narrower, which implied that more elastomer components were left behind in the spherulites as shown in Figure 10(g–i).

During the crystallization process, the amorphous polymer (PPOc) is rejected from the crystal growth front. As a result, the amorphous component is effectively rejected into interlamellar regions or diffused away from the crystal front. However, if the diffusion rate of the amorphous molecules is much lower than growth rate of spherulites, then there could be amorphous

domain build up in front of the crystal growth front. Also, if the LLPS has left some large amorphous domains (droplets) in the crystal growth front, then those droplets will be trapped inside the spherulites.

CONCLUSIONS

The kinetics of LLPS and crystallization were investigated for iPP/PPOc alloy. The liquid–liquid phase separation exerted a significant influence on the crystallization behavior. Quantities such as nuclei density and overall rate of crystallization were strongly dependent upon LLPS process. Comparing to crystallization directly from an isotropic melt, crystallization from a previously phase-separated molten blend resulted in lower crystallization temperature, slower crystallization rate and smaller nuclei density. In contrast, the melting temperature and crystallinity did not show any obvious difference between the two quench procedures as they should be. The phase separation process also had a significant effect on the size and distribution of rubber phase in iPP matrix, and the morphology of spherulites boundary. Those results suggest that LLPS had significant effect on the crystalline structure development in such polymer alloy.

ACKNOWLEDGMENTS

This work was supported by National Natural Science Foundation of China (No. 50930003) and Young Scientist Fund of NSFC (No. 21004071).

REFERENCES

1. Galli, P.; Haylock, J. C. *Prog. Polym. Sci.* **1991**, *16*, 443.
2. Tullo, A. H. *Chem. Eng. News* **2001**, *79*, 10.
3. Nedorezovaa, P. M.; Chapurina, A. V.; Koval'chuka, A. A.; Klyamkinaa, A. N.; Aladysheva, A. M.; Optova, V. A.; Shklyarukb, B. F. *Polymerization* **2010**, *52*, 121.
4. Quijada, R.; Guevara, J. L.; Galand, G. B.; Rabagliati, F. M.; Lopez-Majada, J. M. *Polymer* **2005**, *46*, 1567.
5. Rulhoff, S.; Kaminsky, W. Macromol. *Chem. Phys.* **2006**, *207*, 1450.
6. Zhang, C. H.; Shang, Y. G.; Chen, R. F.; Zheng, Q. J. *Appl. Polym. Sci.* **2011**, *119*, 1560.
7. Crist, B.; Hill, M. J. J. Polym. *Sci. Part B: Polym. Phys.* **1997**, *35*, 2329.
8. Zhang, X. H.; Wang, Z. G.; Muthukumar, M.; Han, C. C. Macromol. *Rapid Commun.* **2005**, *26*, 1285.
9. Matsuba, G.; Shimizu, K.; Wang, H.; Wang, Z. G.; Han, C. C. *Polymer* **2003**, *44*, 7459.
10. Di Lorenzo, M. L. *Prog. Polym. Sci.* **2003**, *28*, 663.
11. Mohammad, R. N.; James, N. H. J. *Appl. Polym. Sci.* **2007**, *104*, 634.
12. Wenig, W.; Meyer, K. Colloid Polym. *Sci.* **1980**, *258*, 1009.
13. Blom, H. P.; Teh, J. W.; Bremner, T.; Rudin, A. *Polymer* **1998**, *39*, 4011.
14. Bartczak, Z.; Gabski, A.; Martuscelli, E. Polym. *Eng. Sci.* **1984**, *24*, 1155.
15. Yokoyama, Y.; Ricco, T. J. *Appl. Polym. Sci.* **1997**, *66*, 1007.
16. Shangguan, Y. G.; Song, Y. H.; Zheng, Q. *Polymer* **2007**, *48*, 4567.
17. Martuscelli, E.; Sylvestre, C.; Bianchi, L. *Polymer* **1983**, *24*, 1458.
18. Feng, Y.; Hay, J. N. *Polymer* **1998**, *39*, 6723.
19. Fan, Z.; Zhang, Y.; Xu, J.; Wang, H.; Feng, L. *Polymer* **2001**, *42*, 5559.
20. Xu, J.; Fu, Z.; Fan, Z.; Feng, L. Eur. *Polym. J. 2002*, 38, **1739**.
21. Zhang, Y.; Fan, Z.; Feng, L. J. *Appl. Polym. Sci.* **2002**, *84*, 445.
22. Fu, Z.; Fan, Z.; Zhang, Y.; Feng, L. *Eur. Polym. J.* **2003**, *39*, 795.
23. Cai, H.; Luo, X.; Ma, D.; Wang, J.; Tan, H. J. *Appl. Polym. Sci.* **1999**, *71*, 103.
24. Prentice, P. *Polymer* **1982**, *23*, 1189.
25. Besomles, M.; Menguel, J.-F.; Delmas, G. J. Polym. *Sci. Part B: Polym. Phys.* **1988**, *26*, 1881.
26. Karger-Kocsis, J.; Kiss, L.; Kuleznev, V. N. Polym. *Commun.* **1984**, *25*, 122.
27. Cheng, S. Z. D. Phase Transitions in Polymers: The Role of Metastable States; Elsevier: Amsterdam, **2008**; p 266.
28. Wang, J. H.; Niu, H.; Dong, J. Y.; Du, J.; Han, C. C. *Polymer* **2012**, *53*, 1507.
29. Dong, J.; Zhu, F.; Han, C. C., et al. China Pat CN1982341 (**2007**).
30. Müller, A. J.; Hernández, Z. H.; Arnal, M. L.; Sánchez, J. J. Polym. *Bull.* **1997**, *39*, 465.
31. Virkkunen, V.; Laari, P.; Pitkänen, P.; Sundholm, F. *Polymer* **2004**, *45*, 3091.
32. Xu, J. T.; Feng, L. X.; Yang, S. L.; Wu, Y. N.; Yang, Y. Q.; Kong, X. M. *Polymer* **1997**, *38*, 4381.
33. Xu, J. T.; Ding, P. J.; Fu, Z. S.; Fan, Z. Q. Polym. *Int.* **2004**, *53*, 1314.
34. Zhang, X. H.; Wang, Z. G.; Muthukumar, M.; Han, C. C. *Macromol. Rapid Commun.* **2005**, *26*, 1285.
35. Zhang, X. H.; Man, X. K.; Han, C. C.; Yan, D. D. *Polymer* **2008**, *49*, 2368.
36. Martuscelli, E. Polym. *Eng. Sci.* **1984**, *24*, 563.
37. Martuscelli, E.; Silvestre, C.; Abate, G. *Polymer* **1982**, *23*, 229.
38. Zheng, Q.; Shangguan, Y. G.; Yan, S. K.; Song, Y. H.; Peng, M.; Zhang, Q. B. *Polymer* **2005**, *46*, 3163.
39. Yamada, K. *Macromolecules* **2003**, *36*, 4790.
40. Yeh, P. L.; Birley, A. W.; Hemsley, D. A. Polymer **1985**, *26*, 1155.